International Journal of Mechanical, Industrial and Aerospace Sciences
ISSN: 2517-9950
Vol:6, No:7, 2012

One-Dimensional Numerical Investigation of a Cylindrical Micro-Combustor Applying Electrohydrodynamics Effect

Behrouzinia P., Irani R. A., Saidi M.H.

***Abstract*—**In this paper, a one-dimensional numerical approach is used to study the effect of applying electrohydrodynamics on the temperature and species mass fraction profiles along the micro-combustor. Premixed mixture is H_2-Air with a multi-step chemistry (9 species and 19 reactions). In the micro-scale combustion because of the increasing ratio of area-to-volume, thermal and radical quenching mechanisms are important. Also, there is a significant heat loss from the combustor walls. By inserting a number of electrodes into micro-combustor and applying high voltage to them corona discharge occurs. This leads in moving of induced ions toward natural molecules and colliding with them. So this phenomenon causes the movement of the molecules and reattaches the flow to the walls. It increases the velocity near the walls that reduces the wall boundary layer. Consequently, applying electrohydrodynamics mechanism can enhance the temperature profile in the micro-combustor. Ultimately, it prevents the flame quenching in micro-combustor.

***Keywords*—**micro-combustor,electrohydrodynamics, temperature profile, wall quenching

I. Introduction

IN the recent researches, many MEMS-based (Micro Electromechanical Systems) devices such as micro gas turbines [1], micro reciprocating engines [2], micro thermophotovoltaic systems [3, 4], micro fuel cells [5] etc. need a high-density micro-power supply to operate. Micro combustion is one of the best ways to provide this power. The superiority of this micro-power source to conventional batteries is its higher energy density in comparison with batteries. One of the basic components of a micro-power system is the micro combustor that uses the oxidant-fuel mixture to release desired energy. In the present work, because of high area-to-volume ratio, both thermal and radical quenching mechanisms are important. Fernandez-Pello [6] reviewed some of the technological details related to micro combustion and micro power generation devices. Modeling and simulation of the micro-scale combustion systems has been discussed by many researches recently. Although Li et al [7] concluded that the reacting flow in the micro scale combustion is 2D in nature, but 1D simulation is used in many researches to evaluate the effect of different parameters on micro scale combustion.

P. Behrouzinia is the M.Sc. student with the Mechanical Engineering Department, Sharif University of Technology, Tehran, Iran (e-mail: pooya_behroozinia@mech.sharif.edu).

A. Irani R. is the Ph.D. student with the Mechanical Engineering Department, Sharif University of Technology, Tehran, Iran (e-mail: abirani@mech.sharif.edu).

M.H. Saidi is the Professor of the Mechanical Engineering Department, Sharif University of Technology, Tehran, Iran (P.O. Box 11155-9567, e-mail: saman@ sharif.edu).

Also, Kaisare and Vlachos [8] showed that the results of both the 1D and 2D numerical simulation are in good agreements. Li et al [9] developed a 1D model to demonstrate the effect of combustor size, fuel property, fuel-air equivalence ratio and unburned mixture temperature on the heat loss ratio and heat recirculation ratio. They concluded that the hydrogen is more suitable in comparison with the methane and propane due to its higher flame temperature and thinner flame thickness.

Another key issue of this work is electrohydrodynamics (EHD). Bushnel [10] and Malik et al. [11] reported several ionic wind velocities affected drag reduction. Soetomo [12] demonstrated experimentally that induced AC and DC corona discharge along a flat plate, in the case of flow velocities up to 2 m/s, results in the drag reduction. Soldati [13] observed numerically that increasing EHD flow intensity reduces the drag. Also, the heat transfer enhancement in natural convection by using EHD initiated in 1962 by Lykoudis and Yu [14]. They studied natural convection between a cold cylinder and a hot wire at center of cylinder. Also, they applied a non-uniform electric field. They concluded that heat transfer enhances with secondary flow produced by electric force. Yabe et al. [15] developed a model for investigation of the dissolution and the experimental corona wind effect. In their research, they used an slender wire for anode and a plate for cathode. They observed that there are positive ions in the whole of the region except near hot wire. They estimated electric potential by numerical methods. Consequently, they showed that the corona wind produced by Coulomb force induced to ions and natural gas molecules.

In the present work, a 1D numerical method is used to investigate EHD application affecting combustion in micro scales. A home-made 1D transient code is developed to do simulations. The burning mixture is H_2–air with a detailed reaction mechanism of 9 species and 19 reactions. Furthermore, heat transfer with the surrounding along the combustor walls is considered. Temperature and species mass fraction profiles are plotted for different heat transfer coefficients and different number of electrodes at steady state condition. As can be seen from the results of the present work, they used to locate the flame zone in micro-scales. Also, effect of various parameters on thermal behavior of a micro combustor can be compared and only highly effective of them choose to design. For example in many applications, generating heat near the region of interest is important in devices. Consequently, locating the point with the highest temperature is desired [21]. This phenomenon is similar to a jet with low velocity flows to earth electrode and applicable to complex geometries for enhancing heat transfer.

In this method, there are no excess sound, vibration and spark. Corona can be in the form of radiation or flowing with the effect of exerting positive voltage. Flowing form almost occurs when high or low voltage exerts that there is ionization state but radiation form occurs when medium voltage exerts and it observes in the steady state flows. Negative voltage results are different with these results completely, however, since positive voltage lead to phenomenon becomes stable and also has many application, almost it used in research. In high powers, joule heating that converts electric energy to heat energy leads to reduction the efficiency. Fig. 1 shows the physics of the corona mechanism.

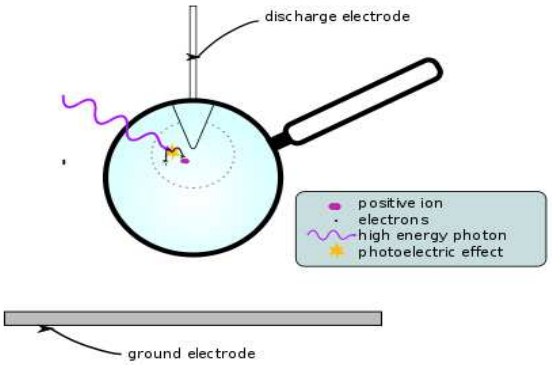

Fig. 1 Corona discharge initiation [19]

Corona wind leads to riot the boundary layer and consequently improves the heat transfer in the micro-combustor which prevents wall quenching. This phenomenon called EHD-enhanced heat and mass transfer. EHD Advantages are as follow:

i. Implementation of this method is simple and only needs one electric converter and electrodes.
ii. Heat and mass transfer coefficients can regulate simply by electric field intensity.
iii. In many applications consumption of electric energy is low.

Positive and negative corona mechanisms seem like together. A natural atom or molecule in the region with high electric field (for example a region with high electric potential near the sharp electrode) ionized by an external motive (for example photon interactions). Fig.2 shows corona mechanism.

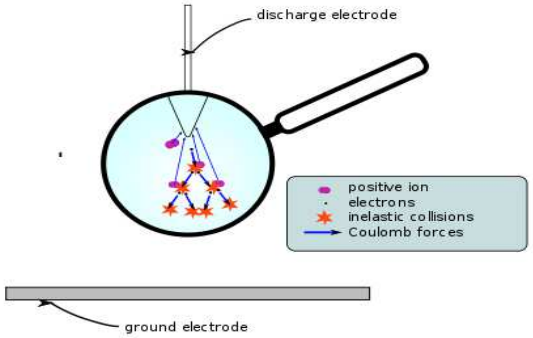

(a)

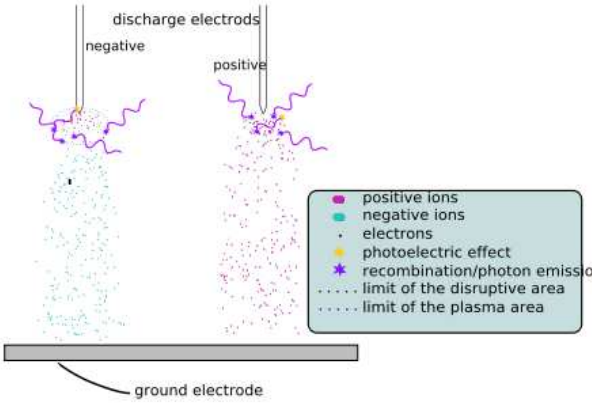

(b)

Fig. 2 (a) Electrical breakdown; (b) recombination and upkeep of the discharge [19]

So electric field affects these ionized particles and prevents the adhesion of particles together. Moreover, it can accelerate the particles which enhance the kinetics energy. With effect of energized electrons with high charge to mass ratio and high acceleration, a number of produced ions impact to natural atoms. This chain continues when an electron avalanche produces. The positive and the negative corona are based on this electron avalanche.

Positive corona initiates from the region with high electric potential. In this type, the sharp electrode has positive voltage and the electrode with lower curvature has ground voltage. The ionized Electrons move to the electrode with high curvature.

In the positive corona, the production of the secondary electrons for avalanche is continuing in the fluid and in the region out of the plasma. The electrons which are produce by the ionization of natural gas molecules attract to sharp electrode and plasma. Therefore, many avalanches produce.

Positive corona region has two sections. One of these sections is the Inner region. This region involves positive ions, electron, electron avalanche and plasma. The outer region is the other section of positive corona that involves a number of positive ions with low velocity moving to positive electrode.

The two regions have a common zone. In this zone secondary electrons that produced by photons exited by plasma move to plasma region. Inner region called plasma region and outer region called one-pole.

Establishment of negative corona is more complex than positive corona. This type of corona also initiates by production of external ionization. Ionized Electrons with natural gas, are unsuitable for production of secondary electrons that produce electron avalanche; because these electrons move to positive electrode. However, for negative corona the way of production of the secondary electrons is photoelectric phenomenon from electrode surface. Energy source for released electrons is photon with high energy.

Principle difference between positive and negative corona is the method of producing secondary electrons. In the positive corona, secondary electrons produce by gases around the

plasma region and released electrons move to plasma, but in the negative corona, they are produced by electrode and move out.

Negative corona can divide by three regions. In the inner region high energized electrons impact with natural atoms and cause production of the electron avalanche. In the outer region the negative ions produced. In the middle region, there is no sufficient energy to produce the electron avalanche, but it is a partition of plasma and has plasma properties. Inner region is the ionized plasma and the middle region is non-ionized plasma. Also, outer region is one-charge region.

II. Computational Domain, Formulation and Solution Method

A. Computational Domain

In this study, a cylindrical reactor is used as shown schematically in Fig. 3.

As can be seen from the Fig. 3, the combustor diameter is very small in comparison with the reactor length, therefore the temperature in radial direction is assumed to be constant. Therefore, it is in good agreement with the 1D assumption. The heat transfer to the upstream by the solid wall conduction is neglected in the present work.

In this work, one and two electrodes have been used in combustor transversely that electrode positions are from outward of plane toward in the plane. Electrodes are shown in the Fig.3 with bold points at center of combustor.

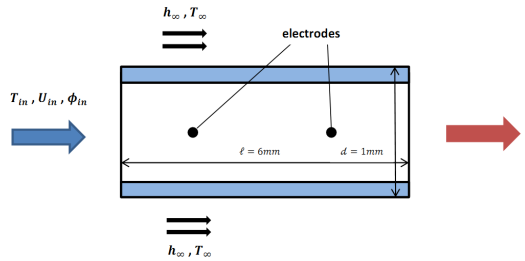

Fig. 3 Schematic of cylindrical reactor and electrodes used in this work

B. Ehd Equations

From electric field and charge density relations due to corona effect, this equation produced:

$$\nabla.(\varepsilon_0 E) = q \tag{1}$$

The relation between electric field density and voltage is:

$$E = -\nabla V \tag{2}$$

And the charge continuity equation is:

$$\nabla.J = 0 \tag{3}$$

Where J is charge density has been obtained from ohm formula:

$$J = qbE + qu \tag{4}$$

Two right hand side terms of (4) are ion movability and charge displacement respectively. From order of magnitude, Ion velocities, bE, are higher order of magnitude compare to the fluid velocity, u. thus, we can relinquish the second right term of (4). Also, (1) combined with (2) and therefore this equation obtained:

$$\nabla^2 V = -\frac{q}{\varepsilon} \tag{5}$$

In addition, if all of these equations combine together, an important equation obtained:

$$q^2 = \varepsilon(\nabla V.\nabla q) \tag{6}$$

Boundary conditions on wire electrodes are:

$$q = q_0 \quad \text{and} \quad V = V_0 \tag{7}$$

Where V_0 is the applied voltage to wire electrodes and q_0 is charge density on surface of wire electrode that obtained from peek formula [20]:

$$q_0 = \frac{l_w J_p}{\pi brf[30\delta + 9(\frac{\delta}{r})^{\frac{1}{2}}]} \times 10^{-5} \tag{8}$$

Where δ is $\frac{T_0 P}{T P_0}$, T_0=293 k, P_0=1.1×[10]^5, T combustor temperature, P combustor pressure, J_p average electric current density on plates, l_w wire to wire distance, b mobility, r corona wire radius and f is roughness. Roughness for clean wires is 1.

Using corona discharge in this work adds a term into the energy equation generally:

$$\frac{\partial T}{\partial t} + \frac{\partial (uT)}{\partial x} = \alpha \frac{\partial^2 T}{\partial x^2} + \frac{qbE^2}{\rho C_p} \tag{9}$$

However, this term adds to special forward energy equations that discuss in next sections.

C. 1D Model Equations and Solution Method

Continuity, energy transport and species mass transport equations in the transient 1D model form an Advection-Diffusion-Reaction (ADR) system of equations. Because we assumed that wall of combustor is inert, the gas radiation and the work of viscous and pressure forces can be neglected. Thus, energy and mass balance equations are as follows:

$$\rho C_p \frac{dT}{dt} + \left(\rho C_p u - \sum_{k=1}^{K} \rho C_{p,k} D \nabla Y_k \right) \nabla T = \nabla.(\lambda \nabla T) - \sum_{k=1}^{K} h_k \dot{w}_k \tag{10}$$

$$\rho \frac{dY_k}{dt} + \nabla(\rho u Y_k) = \nabla(\rho D \nabla Y_k) + \dot{w}_k W \tag{11}$$

In the present work, the flow is laminar and the pressure loss along the combustor is neglected. Also, another assumption of this work is that the reactants and products species are ideal gases. Therefore, density and velocity are obtained from the following equations:

$$\frac{1}{\rho} = \frac{1}{P} R_u T \sum_{k=1}^{K} \frac{Y_k}{W_k} \tag{12}$$

$$u_j = \frac{u_{in}\left(Area\right)_{in}\rho_{in}}{\left(Area\right)_j \rho_j} \quad (13)$$

In the above equations, energy equation, species mass transport equations and reaction rates are coupled to each other. Solution of above system of equations with conventional CFD methods causes some difficulty. In addition, a multi-step chemistry mechanism is used. Thus, the reaction rate calculation results in a stiff system of ODEs. In the present work, to solve these equations simultaneously, the Operator Splitting (OS) method is used. The method of this solution is dividing a system into subsystems that can be integrated in time [16]. Splitting technique has two main schemes: first order scheme (linear), and second or higher order scheme (non-linear). The above equations are non-linear. Therefore, the Strang Splitting method which is preferable for nonlinear stiff system of PDEs, is used. This method divides the nonlinear stiff systems of PDEs into two non-stiff systems of PDEs and two stiff systems of ODEs. Stiff systems of ODEs are solved by VODE method (Variable-coefficient Ordinary Differential Equation) [17]. The solution procedure is as follows:

i. Advection-Diffusion (A-D1): In this step, the solutions are energy and mass balance equations without the reaction terms for the first half of time-step:

$$\rho C_p \frac{dT^*}{dt} + \left(\rho C_p u - \sum_{k=1}^{K} \rho C_{p,k} D \nabla Y_k\right)\nabla T^* = \nabla.\left(\lambda \nabla T^*\right) + qbE^2 \quad (14)$$

$$\rho \frac{dY_k^*}{dt} + \nabla\left(\rho u Y_k^*\right) = \nabla\left(\rho D \nabla Y_k^*\right) \quad (15)$$

Where $t_n < t < t_{n+\frac{1}{2}}$ and initial conditions are as below:

$$T^*\left(t_n\right) = T^n \ , \ Y_k^*\left(t_n\right) = Y_k^n \quad (16)$$

ii. Reaction (R): In this step, with consideration of only the reaction term in the whole time-step, the equations reduce to:

$$\rho C_p \frac{dT^{**}}{dt} = -\sum_{k=1}^{K} h_k \dot{w}_k \quad (17)$$

$$\rho \frac{dY_k^{**}}{dt} = \dot{w}_k W \quad (18)$$

where $t_n < t < t_{n+1}$ and initial conditions are as below:

$$T^{**}\left(t_n\right) = T^*\left(t_{n+\frac{1}{2}}\right), \ Y_k^{**}\left(t_n\right) = Y_k^*\left(t_{n+\frac{1}{2}}\right) \quad (19)$$

iii. Advection-Diffusion (A-D2): This step is similar to step 1, but the flow field is solved for the 2nd half of time-step:

$$\rho C_p \frac{dT^{***}}{dt} + \left(\rho C_p u - \sum_{k=1}^{K} \rho C_{p,k} D \nabla Y_k\right)\nabla T^{***} = \nabla.\left(\lambda \nabla T^{***}\right) + qbE^2 \quad (20)$$

$$\rho \frac{dY_k^{***}}{dt} + \nabla\left(\rho u Y_k^{***}\right) = \nabla\left(\rho D \nabla Y_k^{***}\right) \quad (21)$$

where $t_{n+\frac{1}{2}} < t < t_{n+1}$ and initial conditions are as follows:

$$T^{***}\left(t_{n+\frac{1}{2}}\right) = T^{**}\left(t_n\right), \ Y_k^{***}\left(t_{n+\frac{1}{2}}\right) = Y_k^{**}\left(t_n\right) \quad (22)$$

After all these three steps are solved for one time step, the new solutions are set as the initial conditions of next time-step:

$$T^{n+1} = T^{***}\left(t_{n+1}\right) \ , \ Y_k^{n+1} = Y_k^{***}\left(t_{n+1}\right) \quad (23)$$

The above procedure is repeated iteratively until reaching steady state. To solve the A-D equations, the power-law scheme with an LU decomposition solver is used.

D.Combustion Modeling

A multi-step and general reaction mechanism is considered:

$$\sum_{k=1}^{K} \nu_{ki}^{'} \chi_k \Leftrightarrow \sum_{k=1}^{K} \nu_{ki}^{''} \chi_k \ , \ (i = 1, 2, ...I) \quad (24)$$

The rate of production of each species is:

$$\dot{\omega}_k = \sum_{i=1}^{I} \nu_{ki} q_i \ , \ (k = 1, ..., K) \quad (25)$$

where the right hand side terms are:

$$\nu_{ki} = \nu_{ki}^{'} - \nu_{ki}^{''} \quad (26)$$

$$q_i = \left(\sum_{k=1}^{K} a_{ki}[X_k]\right)\left(k_{fi}\prod_{k=1}^{K}[X_k]^{\nu_{ki}^{'}} - k_{ri}\prod_{k=1}^{K}[X_k]^{\nu_{ki}^{''}}\right) \quad (27)$$

where the forward reaction rate constants calculate from the Arrhenius equation:

$$k_{fi} = A_i T^{\beta_i} \exp\left(\frac{-E_i}{R_c T}\right) \quad (28)$$

The reverse reaction rate constants are:

$$k_{ri} = \frac{k_{fi}}{k_{Ci}} \quad (29)$$

$$k_{Ci} = k_{Pi}\left(\frac{P_{atm}}{RT}\right)^{\sum_{k=1}^{K}\nu_{ki}} \quad (30)$$

$$k_{Pi} = \exp\left[\frac{\Delta S_i^o}{R} - \frac{\Delta H_i^o}{RT}\right] \quad (31)$$

$$\frac{\Delta S_i^o}{R} = \sum_{k=1}^{K} \nu_{ki} \frac{S_k^o}{R} \quad (32)$$

$$\frac{\Delta H_i^o}{RT} = \sum_{k=1}^{K} \nu_{ki} \frac{H_k^o}{RT} \quad (33)$$

$$\frac{S_k^o}{R} = a_{1k}\ln T_k + a_{2k}T_k + \frac{a_{3k}}{2}T_k^2 + \frac{a_{4k}}{3}T_k^3 + \frac{a_{5k}}{4}T_k^4 + a_{7k} \quad (34)$$

$$\frac{H_k^o}{RT_k} = a_{1k} + \frac{a_{2k}}{2}T_k + \frac{a_{3k}}{3}T_k^2 + \frac{a_{4k}}{4}T_k^3 + \frac{a_{5k}}{5}T_k^4 + \frac{a_{6k}}{T_k} \quad (35)$$

The above equations form a stiff system that solved by using VODE method.

E. Thermophysical Properties

In this work, as used by Kaisare and Vlachos research [8], the thermal diffusivity of the gas mixture is assumed to be constant. This value is considered to be. Gas phase thermal conductivity is calculated from the mixture average formula [18]:

$$\lambda = \frac{1}{2}\left(\sum_{k=1}^{K} \lambda_k x_k + \frac{1}{\sum_{k=1}^{K} X_k / \lambda_k} \right) \quad (36)$$

Thermal conductivity of H2, O2, H2O and N2 species is assumed to be a polynomial function of temperature. The polynomial coefficients are curve fitting at the temperature range (300-2200 K). Thermal conductivities of the above species are calculated from below relations:

$$\lambda_{H_2} = 2.66\times10^{-11}T^3 - 5.81\times10^{-8}T^2 + 4.18\times10^{-4}T + 6.6\times10^{-2} \quad (37)$$

$$\lambda_{O_2} = 1.76\times10^{-15}T^4 - 3.67\times10^{-11}T^3 - 1.07\times10^{-8}T^2 + 8.68\times10^{-5}T + 1.79\times10^{-3} \quad (38)$$

$$\lambda_{H_2O} = -1.30\times10^{-11}T^3 + 6.58\times10^{-8}T^2 + 4.51\times10^{-5}T - 1.34\times10^{-3} \quad (39)$$

$$\lambda_{N_2} = 8.43\times10^{-16}T^4 + 1.80\times10^{-11}T^3 - 5.24\times10^{-8}T^2 + 9.75\times10^{-5}T + 8.86\times10^{-4} \quad (40)$$

Also molar heat capacity is obtained from the following equation:

$$\frac{C_{pk}^{o}}{R} = a_{1k} + a_{2k}T_k + a_{3k}T_k^2 + a_{4k}T_k^3 + a_{5k}T_k^4 \quad (41)$$

The above coefficients are similar to the coefficients used in (34) and (35).

III. Results And Discussion

The effect of convective heat transfer coefficient on temperature and mole fractions profiles are investigated in the following three cases. One of these cases is checking the micro-combustor without applying EHD method. Another case is applying EHD method using one electrode in micro-combustor that is located at the center of it and the latter case is applying EHD with two electrodes that are located at one quarter and three quarter of micro-combustor length respectively.

Because of micro-scales domain and to prevent melting of micro-electrodes, applied voltage must not be much high. For this reason, in this study, applied voltage is 2000 volt.

A computational grid independency test is performed. The temperature profile for 71, 141 and 211 nodes are shown in Fig. 4. As can be seen from this result, 141 nodes are preferable number of grids [21].

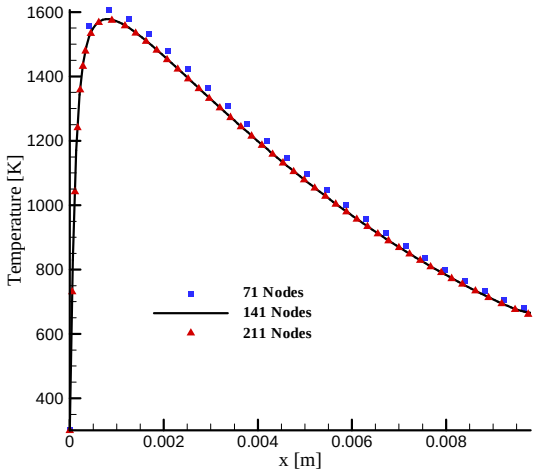

Fig. 4 Temperature profiles for different number of grids [21]

Temperature profiles with different convective heat transfer coefficients (h=5,10,20 W/(m^2.K)) are exhibited in Fig. 5-6. These figures show that applying electrodes can enhance temperature profile and also using two electrodes is better than using one electrode to enhance it. In spite of enhancing heat transfer with EHD method, energy added in micro-combustor by electrodes is high enough that its temperature rises to desirable value. Also, it can be seen that maximum and average temperature along the micro-combustor enhanced using EHD method.

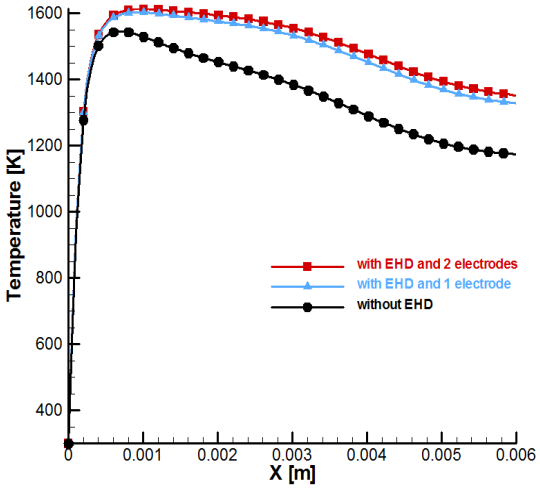

Fig. 5 Temperature profile at h=5 ($\frac{W}{m^2.K}$)

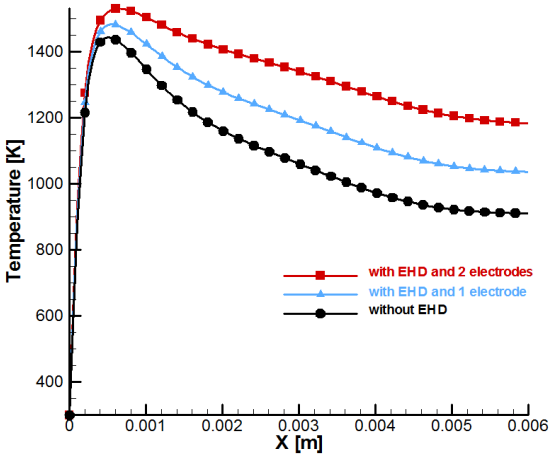

Fig. 6 Temperature profile at h=10 ($\frac{W}{m^2.K}$)

Alternatively, [OH] mole fraction in different convective heat transfer coefficients using three cases are shown in Fig. 8-10. It can be seen that this mole fraction profile is higher in the case of applying EHD than using without EHD method. Also, using two electrodes can increase this profile more than using one electrode.

The average temperatures in the case of h=5 are 1270 K, 1430 K and 1570 K for the case of no EHD, one electrode and two electrodes, respectively. These values in the case of h=10 are 1010 K, 1130 K, 1260 K and in the case of h=20 are 751 K, 914K, 1120 K.

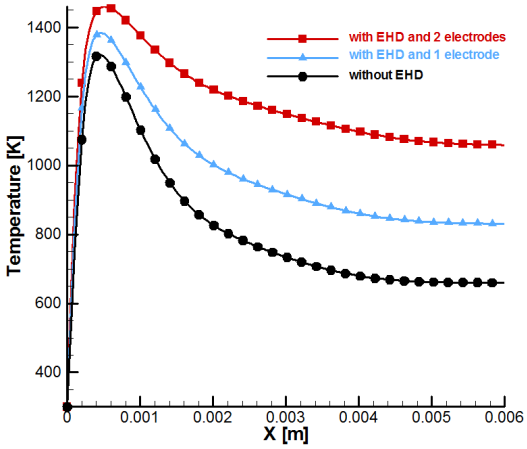

Fig. 7 Temperature profile at h=20 ($\frac{W}{m^2.K}$)

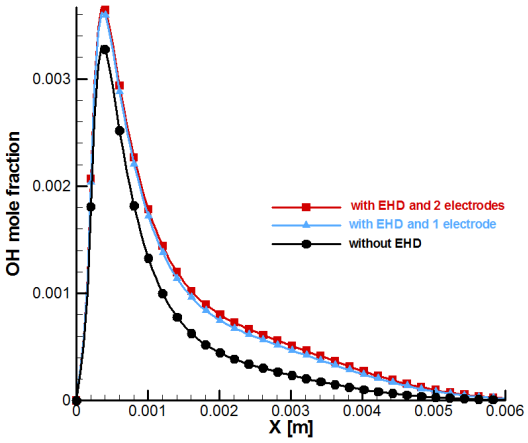

Fig. 8 [OH] mole fraction profile at h=5 ($\frac{W}{m^2.K}$)

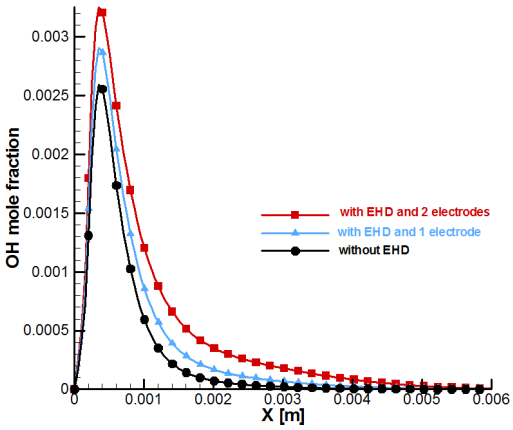

Fig. 9 [OH] mole fraction profile at h=10 ($\frac{W}{m^2.K}$)

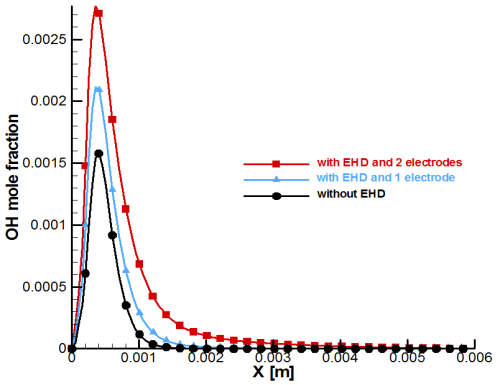

Fig. 10 [OH] mole fraction profile at h=20 ($\frac{W}{m^2.K}$)

Furthermore, $[O_2]$ and $[H_2]$ mole fractions in different convective heat transfer coefficients in aforementioned three cases are shown in Fig. 11-16.

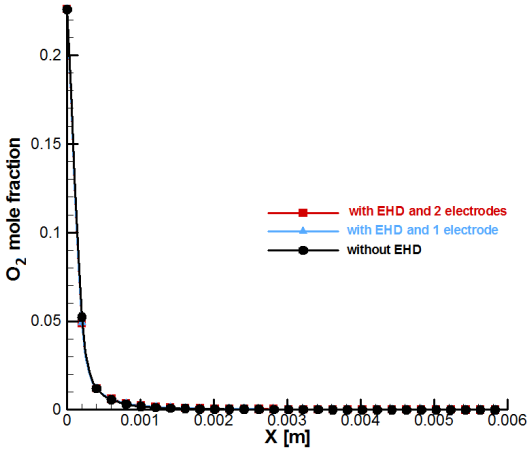

Fig. 11 [O_2] mole fraction profile at h=5 ($\frac{W}{m^2.K}$)

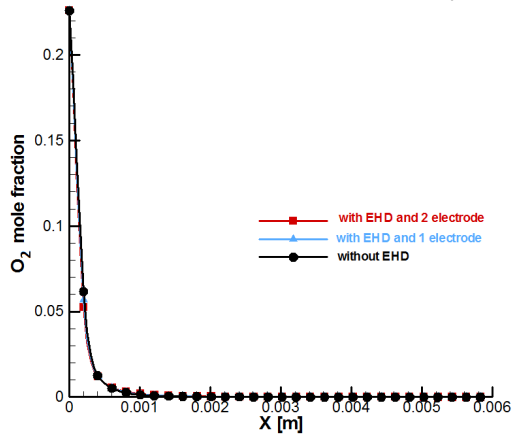

Fig. 12 [O_2] mole fraction profile at h=10 ($\frac{W}{m^2.K}$)

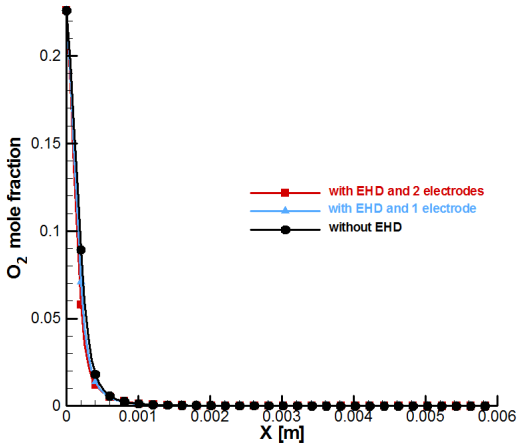

Fig. 13 [O_2] mole fraction profile at h=20 ($\frac{W}{m^2.K}$)

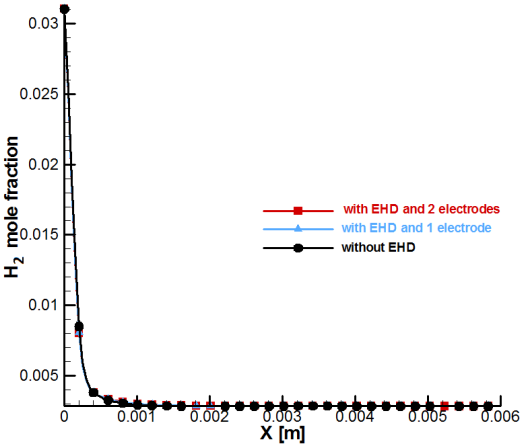

Fig. 14 [H_2] mole fraction profile at h=5 ($\frac{W}{m^2.K}$)

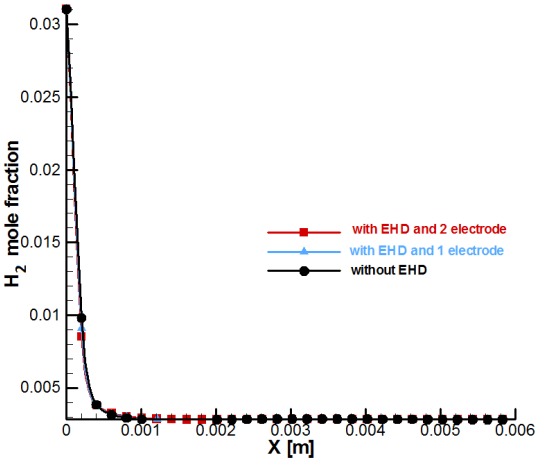

Fig. 15 [H_2] mole fraction profile at h=10 ($\frac{W}{m^2.K}$)

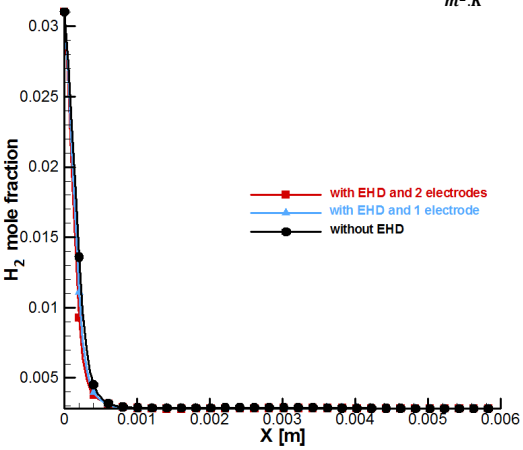

Fig. 16 [H_2] mole fraction profile at h=20 ($\frac{W}{m^2.K}$)

IV. Conclusion

In the present work, one dimensional numerical approach has been studied to investigate the effect of applying EHD method on the micro-combustor temperature profile and flame

quenching. Three cases performed in this work namely using one electrode, two electrodes and the case of no EHD. These cases applied to difference convective heat transfer coefficients. A multi-step chemistry mechanism for H_2-air mixture is considered. Also, the lateral convection heat transfer with the surrounding is considered.

The numerical results show that using EHD method can enhance the maximum and average temperature in the micro-combustor and consequently, prevent flame quenching by this temperature rise along micro-combustor. Also in order to increase temperature profile, applying two electrodes is more effective than one electrode. In addition, [OH] mole fraction profile rises with applying electrodes along micro-combustor. By applying this method, there is no need for using catalyst to prevent flame quenching.

Moreover, results illustrate that flame zone is a thin region that located near the micro-combustor inlet and increasing the convection heat transfer coefficient reduces the temperature and radical species concentrations profiles in the flame zone.

REFERENCES

[1] Waitz I.A., Gauba G. and Yang S.T., 1998, "Combustors for micro-gas turbine engines", Journal of Fluids Engineering, 120 (1998) 109-117.
[2] Jin P., Gao Y.L., Liu N., Tan J.B. and Jiang K., 2006, "Design and fabrication of alumina micro reciprocating engine", Journal of Physics: conference series, 48 (2006) 1471-130.
[3] Lee K.H. and Kwon O.C., 2008, "Studies on a heat-recirculating microemitter for a micro thermophotovoltaic system", Combustion and Flame, 153 (2008) 161-172.
[4] Yang W.M., Chou S.K., Shu C., Xue H., Li Z.W., Li D.T. and Pan J.F., 2003, "Microscale combustion research for application to micro thermophotovoltaic systems", Energy Conversion and Management, 44 (2003) 2625-2634.
[5] Vahabi M. and Akhbari M.H., 2009, "Three-dimensional simulation and optimization of an isothermal PROX microreactor for fuel cell applications", International Journal of Hydrogen Energy, 34 (2009) 1531-1541.
[6] Fernandez-Pello A.C., 2002, "Micro-power generation using combustion: Issues and approaches", Twenty-Ninth International Symposium on Combustion, July 21-26, 2002, Sapporo, Japan.
[7] Li Z.W., Chou S.K., Shu C., Xue H. and Yang W.M., 2005, "Characteristics of premixed flame in microcombustors with different diameters", Applied Thermal Engineering, 25 (2005) 271-281.
[8] Kaisare N.S. and Vlachos D.G., 2007, "Optimal reactor dimensions for homogenous combustion in small channels", Catalysis Today, 120 (2007) 96-106.
[9] Li J., Chou S.K., Li Z. and Yang W., 2008, "Development of 1D model for the analysis of heat transport in cylindrical micro-combustors", Applied Thermal Engineering.
[10] D. Bushnell, Turbulent drag reduction for external flows, AIAA Paper 1983-0231, Reno, USA, January 1983.
[11] M.R. Malik, L. Weinstein, M. Hussaini, Ion wind drag reduction, AIAA Paper 1983-0231, Reno, USA, January 1983.
[12] F. Soetomo, The influence of high-voltage discharge on flat plate drag at low Reynolds number air flow, M. S. Thesis, Iowa State University, Ames, Iowa, 1992.
[13] A. Soldati, S. Banerjee, Turbulence modification by large scale organized electrohydrodynamic flows, Phys. Fluids 10 (7) (1998) 1742–1756.
[14] Lykoudis, P.S., Yu, C.P., 1962, The influence of electrostrictive forces in natural thermal convection, international journal of heat and mass transfer, 6, 853-862.
[15] Yabe, A., Mori, Y., Hijitata, K., EHD study of corona wind between wire and plate electrodes, AIAA J., 16 (1978) 340-345.
[16] Sportisse B., 2000, "An analysis of operating splitting techniques in the stiff case", Journal of Computational Physics, 161, 140–168.
[17] Brown P.N., Byrne G.D. and Hindmarsh A. C., 1988, "VODE, a variable-coefficient ODE solver", SIAM Journal of Scientific and Statistical Computing.
[18] Marthur S., Tondon P.K. and Saxena S.C., Molecular physics, 12:569 (1967).
[19] Junhong Chen, "Direct-Current Corona Enhanced Chemical Reactions", Ph.D. Thesis, University of Minnesota, USA. August 2002.
[20] Peek, F.W., Dielectric Phenomena in high-voltage engineering, McGraw-Hill, New York, (1929).
[21] Irani R. A., Saediamiri M., Saidi M.S., Saidi M.H. and Shafii M.B., "one dimensional numerical investigation of a cylindrical micro-combustor", ASME Summer Heat Transfer Conference July 19-23, 2009, San Francisco, California USA.